

A NEW CLASS OF NONIONIC PHOTOSENSITIVE SURFACTANTS: SOME INSIGHTS CONCERNING CONFORMATIONS

Kenneth A. Smith, T. Alan Hatton, Tiangang Shang, and Brad Ciccirelli
Department of Chemical Engineering, Massachusetts Institute of Technology, Cambridge, MA 02139

Abstract—We report on a new class of nonionic, photosensitive surfactants consisting of a polar di(ethylene oxide) head group attached to an alkyl spacer of between two and eight methylene groups, coupled through an ether linkage to an azobenzene moiety. Structural changes associated with the interconversion of the azobenzene group between its cis and trans forms as mediated by the wavelength of an irradiating light source cause changes in the surface tension and self-assembly properties. Differences in saturated surface tensions (surface tension at concentrations above the CMC) were as high as 14.4 mN/m under radiation of different wavelengths. The qualitative behavior of the surfactants changed as the spacer length changed, attributed to the different orientations adopted by the different surfactants depending on their isomerization states, as revealed by neutron reflection studies. The self-assembly of these photosensitive surfactants has been investigated by light scattering, small angle neutron scattering, and cryo-TEM under different illuminations. The significant change in the self-assembly responding to different illumination conditions was attributed to the sign change in Gaussian rigidity, which originated from the azobenzene photoisomerization.

Index Terms—azobenzene, photosensitive surfactants, surface tension

I. INTRODUCTION

Surface tension plays a significant role in many practical applications, including coating processes, detergency, waterproofing of fabrics, and lithography in the microelectronics industry[1]. More recently, surface tension has been shown to be important in emerging high technologies, and can be exploited in the pumping and control of flow in microfluidic devices, and in the microchemical analysis of complex fluids, flow cytometry, rapid DNA screening, etc[2]. Advances in these new technologies will depend strongly on the availability of flexible methods for adjusting and controlling surface tension dynamically. Photo-control using photosensitive surfactants is a potentially attractive route to accomplishing many of the tasks required in these processes. One class of such surfactants is based on the photo-responsive azobenzene group[3, 4], which changes its conformation reversibly when illumination is switched between UV and visible light (Figure 1). Under UV light irradiation,

azobenzene adopts the cis conformation. On illumination with visible light, its conformation reverts back to the trans form[5]. When these azobenzene groups are incorporated within the tail group of a surfactant, this reversible photoisomerization often induces changes in interfacial properties, such as surface tension, and in related bulk solution properties, such as micelle formation and structure. In some applications, however, these systems will be useful only if the changes in surface tension with changing illumination conditions are large, and if the surfactants are used at concentrations well above their critical micelle concentrations (CMCs) so that loss of surfactant by adsorption to interfaces and surfaces does not appreciably affect the bulk properties or surface tensions.

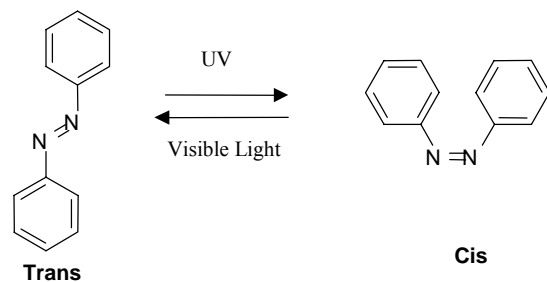


Fig. 1. Photoisomerization of azobenzene.

Several photo-responsive surfactants which show significant changes in critical micelle concentrations (CMCs) and aggregation behavior upon radiation with light of different wavelengths have been reported in the literature [6-9] but in no case did their saturated surface tensions (i.e., surface tension at concentrations well above the CMC) differ from each other by more than 3 mN/m, and in most cases the differences were much smaller, or even negligible. These surfactants do not, therefore, fulfill the requirements for some potential applications, and there is scope for the development of new surfactants that will satisfy these needs. A recent exception is the work of Eastoe et al.[10], who observed surface tension changes of as much as 12 mN/m in photoresponsive stilbene-containing Gemini surfactant systems. Interpretation of their results is somewhat complicated, however, by the competition between simple photoisomerization of the surfactants and dimerization, which leads to non-standard surface tension curves.

Here we report the synthesis of a new class of photoresponsive surfactants that exhibits the large change

in saturated surface tension. Their surface tension and self-assembly properties are also investigated and reported here.

II. EXPERIMENTAL SECTION

A. Synthesis

The photoresponsive surfactants triethylene glycol mono(4-butylazobenzene) ether ($C_4AzoOC_2E_2$), diethylene glycol mono(4',4'-butyloxy, butyl-azobenzene) ($C_4AzoOC_4E_2$), diethylene glycol mono(4',4'-hexyloxy, butyl-azobenzene) ($C_4AzoOC_6E_2$) and diethylene glycol mono(4',4'-octyloxy, butyl-azobenzene) ($C_4AzoOC_8E_2$) (Figure 2) were synthesized according to the procedure in our previous work [11].

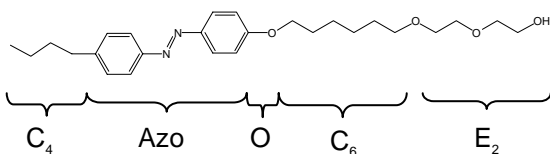


Fig. 2. Molecular structure of photo-responsive surfactants $C_4AzoOC_nE_2$; the structure for $n = 6$ is shown. C_4 = butyl tail group; Azo = azobenzene group; O = ether oxygen middle polar group; C_6 = alkyl spacer with 6 methylene groups; E_2 = surfactant head group consisting of two ethylene oxide moieties.

B. Kinetics of Photo-isomerization

The kinetics of photo-isomerization under continuous illumination was investigated by irradiating a surfactant solution with a continuous narrow band photon flux, and monitoring the trans and cis absorption bands until the system reached its photostationary equilibrium.

C. Surface Tension Measurement

The equilibrium surface tension was measured at a temperature of 25 °C with a Krüss K10T tensiometer using the Wilhelmy plate method. A chart recorder was used to trace the surface tension variation with time.

D. Static Light Scattering (SLS)

Static light scattering experiments were performed at 25 °C using a Brookhaven 200SM goniometer, a BI-9000AT digital autocorrelator, and a Spectra-Physics Argon laser operating at 514 nm.

E. Small Angle Neutron Scattering (SANS)

Neutron scattering intensities were measured as a function of scattering angle on the NG3 30 m SANS line at the National Institute of Standards and Technology (NIST) in Gaithersburg, MD. An unpolarized neutron beam with a wavelength of 6 Å (wavelength spread $\Delta\lambda/\lambda \sim 0.11$) was

used in all experiments. The Q range covered in the experiment was $0.005 < Q < 0.4 \text{ \AA}^{-1}$. Trans samples were measured under ambient light environment. The cis samples were illuminated under UV light (Oriel 6283) for 2 hours before measurement to ensure conversion of all trans surfactants to the cis form.

F. Cryogenic Transmission Electron Microscopy (Cryo-TEM)

The replica cryo-TEM samples were prepared through the QFDE (quick freeze-deep etch) method. The vitrified cryo-TEM samples were prepared in a controlled environment vitrification system (CEVS) and examined by Paul Johnson of the University of Rhode Island. For all processes, trans samples were prepared under ambient light, while cis samples were first illuminated for 2 hours under UV light, and then prepared in the dark.

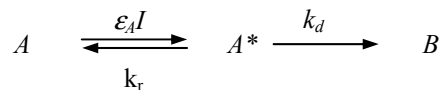
G. Neutron reflection measurement

Neutron reflection experiments were conducted on the NG7 reflectometer at NIST. The samples were placed into a Teflon trough and stabilized for about 60 minutes before measurement. Neutrons with fixed 4.76 Å wavelength were used to illuminate the sample surface. The reflectivities were measured at room temperature and at different incident angles, which correspond to the Q range from 0.05 Å⁻¹ to 0.2 Å⁻¹. The reflectivities from two deuterated $C_4AzoOC_6E_2$ species, azobenzene deuterated and spacer deuterated, were measured in NRW (null reflection water) and pure D₂O, and under both UV and visible illumination, respectively.

III. RESULTS AND ANALYSIS

A. Kinetics of Photo-isomerization

Typical results of photokinetic experiments for an aqueous 0.02 mM solution of $C_4AzoOC_6E_2$ under UV and visible light, with a path length of 10 mm are shown in Figure 3. The kinetics of photoisomerization were analyzed quantitatively by assuming that the absorption of photons of a particular wavelength by an isomer A leads to the excitation of this species to A^* , which can then revert back to A, or transform to species B, according to



where ϵ_A is the molar absorption coefficient and I is the local illumination intensity. The rate constants of reversion to A and conversion to B are k_r and k_d , respectively. In general, the intensity I will depend on the position within the vial owing to absorption by both A and B within the solution. Since the concentrations of these two species were low, however, and since the path length was short, the fraction of incident photons absorbed was small, and I ($\approx I_0$) can be assumed to be constant.

Under the quasi-steady-state assumption that $d[A^*]/dt \sim 0$, and the initial conditions that at $t = 0$, $[\tilde{A}] = 1$, the solution is given by

$$[\tilde{A}] = e^{-\varepsilon_A I_0 \phi t} \quad (1)$$

where $\phi = k_d / (k_d + k_r)$ is the quantum efficiency, reflecting the fraction of excited species that leads to the final product; $[\tilde{A}] = [A]/[A]_0$ is dimensionless concentration of species A .

The kinetic curves for $C_4AzoOC_6E_2$ undergoing trans-to-cis and cis-to-trans conversions under similar illumination intensities of 1.1×10^{-4} mol photons (330 nm)/ m^2 s and 1.3×10^{-4} mol photons (440 nm)/ m^2 s, respectively, are shown in Figure 3. For the trans-to-cis conversion, it can be inferred from data fitting that the quantum efficiency is close to unity, that is, $\phi \cong 1$. For the cis-to-trans isomerization, however, the quantum efficiency was found to be 0.69. The different quantum efficiencies determined here may reflect different reaction mechanisms in these two photoisomerization processes because of geometrical differences in both the excited and the ground states.

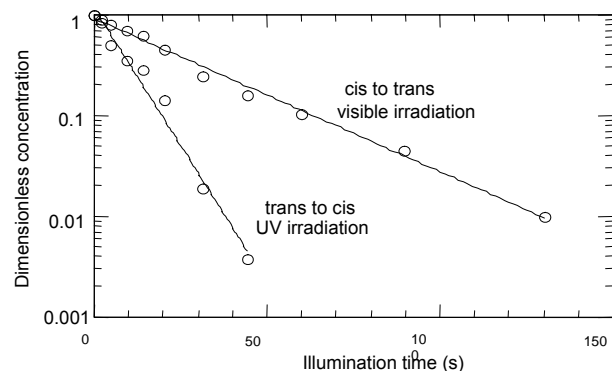


Fig. 3. Kinetics of photo-isomerization in $C_4AzoOC_6E_2$ solutions for the trans-to-cis and cis-to-trans processes under similar irradiation intensities. Solid lines represent least squares fits of the kinetic model to the data.

B. Contact Angle Measurements

The change in surface tension upon changing illumination conditions is reflected in changes in the contact angle of a droplet of the solution on a hydrophobic surface according to the Young Equation[1]

$$\gamma \cos \theta = \gamma_{SV} - \gamma_{SL} \quad (2)$$

where γ_{SV} and γ_{SL} are the surface energies at the solid-vapor and solid-liquid interfaces, respectively.

We show in Figure 4(a) photographs of a droplet of 0.08 mM $C_4AzoOC_6E_2$ solution on a hydrophobic glass surface coated with octadecyl trichlorosilane (OTS) with the surfactants in both the trans and the cis configurations. The equilibrium contact angle of trans surfactant was determined using a goniometer to be 35.8° . In cis form, the contact angle is 53.5° . The contact angle variation with changing light conditions was shown to be reversible.

The time-course of the contact angle variation upon changing illumination is shown in Figure 4(b). There was an initial lag of approximately 40s before significant changes in contact angle were evident. This is somewhat slower than Figure 3 would suggest, but the photon flux was also significantly lower. Following this lag period, the variation with time followed typical exponential approach to equilibrium indicative of a first order process.

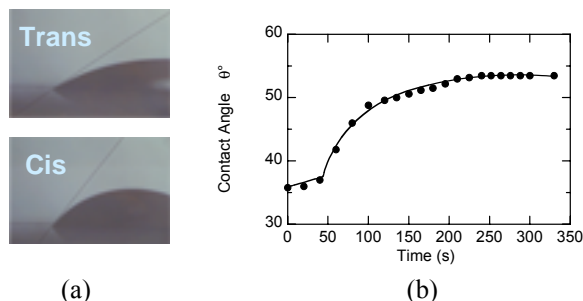


Fig. 4. Contact angle changes for droplets of $C_4AzoOC_6E_2$ solutions (0.07 mM) on a hydrophobic surface under different illumination conditions (visible illumination for the trans isomer, UV illumination for the cis isomer). The time-course of contact angle variation under UV illumination is shown.

C. Surface Tension Measurements

Equilibrium surface tensions, γ , of all aqueous surfactant solutions were measured at different surfactant concentrations before and after UV illumination. The raw results are shown using open symbols in Figure 5, which

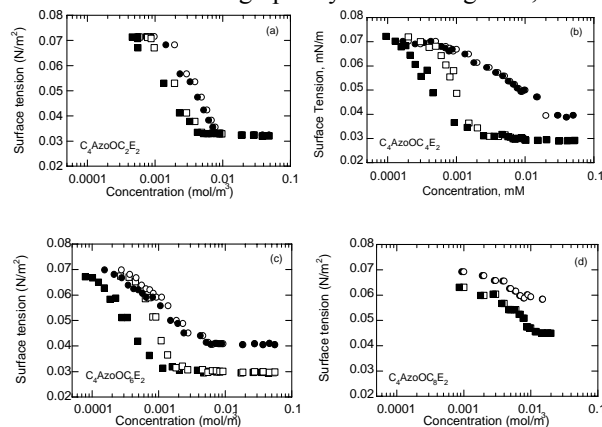


Fig. 5. Concentration dependence of the equilibrium surface tension for photoresponsive surfactants at 25 °C under both visible (squares) and UV light (circles) illumination. The open symbols represent the original data as a function of the nominal, as-prepared concentration; the solid symbols represent data corrected for interfacial adsorption to give the true bulk concentration. (a) $C_4AzoOC_2E_2$ (b) $C_4AzoOC_4E_2$ (c) $C_4AzoOC_6E_2$ (d) $C_4AzoOC_8E_2$

give the surface tension as a function of the nominal or as-

prepared concentration of the solution added to the measurement trough. In many cases, the moles of surfactant adsorbed at the air-water interface constituted a significant proportion of the total number of moles introduced to the

measurement trough, however, so that the true bulk concentration C_b was less than the nominal concentration C_{nom} by an amount determined by the mass balance equation

$$C_b = C_{nom} - \frac{A}{V}\Gamma \quad (3)$$

where A/V is the ratio of the gas-liquid interfacial area to sample volume in the surface tension measurement and Γ is the surface excess concentration in moles per unit area. We have accounted for this surface adsorption effect to estimate the true bulk concentration using procedures detailed below, and show the surface tension as a function of the true bulk concentration using solid symbols in Figure 5.

D. Estimation of True Bulk Concentration and Surface Excess Properties

The true bulk and surface excess concentrations were estimated by using a model developed to relate the surface tension, surface excess concentration and true bulk concentration to the nominal bulk concentration and extracting the appropriate model parameters by least-squares regression of this model on the experimental data.

We relate the surface excess concentration to the true bulk solution concentration through the Frumkin isotherm[12],

$$kC_b = \frac{\Gamma}{\Gamma_\infty - \Gamma} \exp\left[-2\left(\frac{h}{RT}\right)\frac{\Gamma}{\Gamma_\infty}\right] \quad (4)$$

where k is the limiting partition coefficient for the surfactant between the interface and the bulk solution at low surface pressure, h is the infinite dilution surface partial molar heat of mixing of the surfactant at the interface, and Γ_∞ the saturation surface excess concentration.

The surface excess concentration, Γ , of the surfactant in the region prior to micellization is related to the slope of the surface tension curve with respect to the true bulk concentration through the Gibbs adsorption isotherm[1]:

$$\Gamma = -\frac{1}{RT} \frac{d\gamma}{d \ln c} \quad (5)$$

where R is the gas law constant and T the absolute temperature. This equation can be integrated directly to yield the surface tension as a function of the surface excess concentration by applying the Frumkin isotherm to eliminate the true bulk concentration[12]:

$$\gamma = \gamma_0 + \Gamma_\infty RT \left[\ln\left(1 - \frac{\Gamma}{\Gamma_\infty}\right) + \frac{h}{RT} \left(\frac{\Gamma}{\Gamma_\infty}\right)^2 \right] \quad (6)$$

where γ_0 is the surface tension of pure water, i.e., 72 mN/m.

Equations (4), (5) and (6) relate the surface tension and the true bulk concentration to the nominal bulk concentration parametrically through the surface excess concentration. Thus, for a given set of data relating experimental surface tension values to the nominal concentration, we extracted the appropriate model parameters by least squares regression of the model on the data, and developed the true surface tension versus bulk concentration curves, and the true surface excess concentrations.

E. Light Scattering

The self-assembly structure of the surfactant $C_4AzoOC_6E_2$ was investigated by static light scattering. The light scattering results are shown in Figure 6. The linear behavior in $Q^2I(Q)$ vs. Q at the high Q range indicated the rod-like structure for which[13],

$$I(Q) \propto \frac{\pi}{QL} - \frac{2}{(QL)^2} \text{ i.e., } Q^2I(Q) \propto \frac{\pi Q}{L} - \frac{2}{L^2} \quad (7)$$

in which L is the length of the rod or, more precisely, the persistence length. The length of rod is the ratio of the slope to the intercept in the $Q^2I(Q)$ vs Q plot. The persistence lengths for all samples are summarized in Table 1.

Scattering intensities for the 69.4 and 170.0 μM samples showed a qualitatively different behavior in the low Q range from those at 1.72 and 2.35 μM , in which the $Q^2I(Q)$ curve decreases rather than increases in the low Q range. This trend implies the structure of a branched polymer, in which the scattering intensity is described by equation (8)[13],

$$\frac{1}{I(Q)} \propto \frac{3-m}{4M_0} + \frac{Q^2 \bar{l}^2 z}{12M_0} \quad (8)$$

in which m is the number of branches, z is the number of segments in each branch, \bar{l}^2 is the average of the square of the length of segments, and M_0 is the molecular weight of a single branch.

For all samples, the scattering intensities $I(Q)$ showed a power law $I(Q) \propto Q^{-a}$ behavior in the intermediate Q range where a is the fractal dimension of the aggregates[13]. This can be seen clearly in the 9.12 μM sample in which an obvious plateau in the intermediate Q range in the $Q^2I(Q)$ vs Q plot indicates $I(Q) \propto Q^{-2}$. The exponents, or fractal dimensions, for all samples are summarized in Table 1. The results of the static light scattering studies are summarized in Figure 7. Over the concentration range under study, surfactants self-assemble into cylindrical “worm-like” micelles with finite persistence length, as indicated by the linearity at large Q in $Q^2I(Q)$ vs Q plot. The persistence length was almost constant over three concentration decades, and consistent with the worm-like micelle picture in which the persistence length is independent of concentration. With increasing concentration, the fractal dimension of the micelles initially

increased rapidly, but then reached a plateau at higher concentrations. This behavior indicates a “micellar growth” phenomenon, in which, with increasing

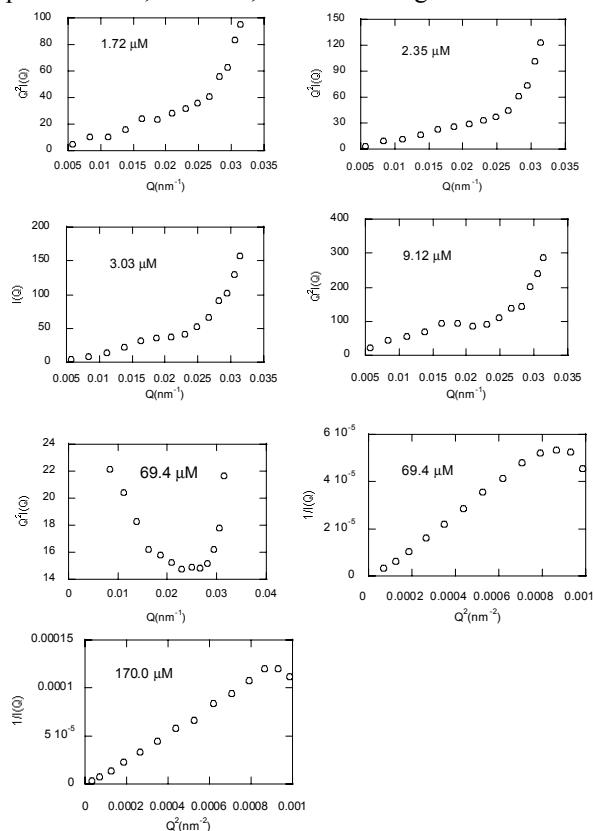


Fig. 6. Light scattering results of $C_4AzoOC_6E_2$. The scattering results are plotted in Kratky Plot for samples of 1.72, 2.35, 3.03, and 9.12 μM , and in Zimm Plot for 69.4 and 170.0 μM samples.

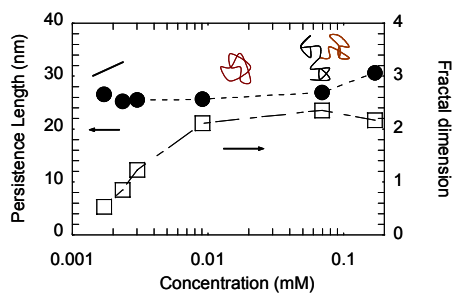


Fig. 7. Summary of static light scattering (SLS) results for trans $C_4AzoOC_6E_2$.

TABLE 1

Summary of Light Scattering Results.

Concentrations (mM)	Persistence length (nm)	Fractal dimension
1.72×10^{-3}	26.6	0.53
2.35×10^{-3}	25.2	0.85
3.02×10^{-3}	25.5	1.23
9.12×10^{-3}	25.6	2.11
69.4×10^{-3}	26.9	2.35
170.4×10^{-3}	30.6	2.17

concentration, more and more surfactant is incorporated into existing micelles to minimize the overall free energy of the system. At low concentrations, micellar growth leads to the appearance of more rigid rods in the individual cylindrical micelles, as indicated by the increase in fractal dimension. When the cylindrical micelle is sufficiently long, it acquires sufficient flexibility to curve into a Gaussian coil, whose fractal dimension is exactly 2. Further increases in concentration lead to elongation of the contour length of the micelle while the Gaussian coil structure is maintained. The retention of the Gaussian coil structure is indicated by the constant fractal dimension of 2 at concentrations above 0.01 mM.

F. Small Angle Neutron Scattering

Typical SANS spectra of both trans and cis samples are shown in Figure 8, for surfactant $C_4AzoOC_6E_2$. It is evident that there are significant differences in the scattering profiles for the two isomers. These significant differences in SANS intensities suggest that the self-assembly behavior may be quite different for the two isomers.

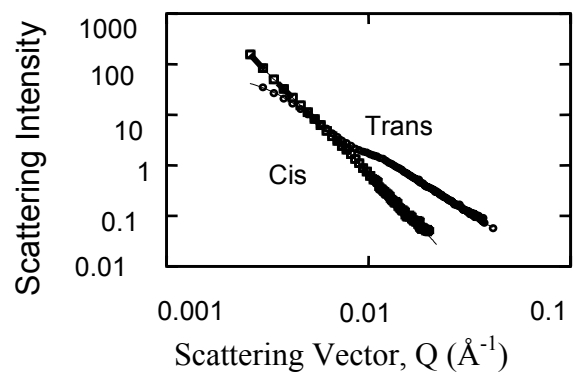


Fig. 8. Small angle neutron scattering results of $C_4AzoOC_6E_2$ 0.6 mM. Open symbols are the experimental data Solid lines represent the model fitting of scattering intensities.

TABLE 2

Fitting Parameters of SANS in Trans Samples.

	$C_4AzoOC_4E_2$	$C_4AzoOC_6E_2$
Concentration (mM)	0.7	1.2
Average vesicular radius (nm)	38.41	43.5
Shell thickness (nm)	11.24	12.5
Polydispersity	0.43	0.37

SANS intensities in the trans samples were found to be described well by the polydispersed vesicle model, in which the core has a well-defined distribution in sizes and the thickness of the shell is fixed[14]. The molecular

lengths of the trans forms of both $C_4AzoOC_4E_2$ and $C_4AzoOC_6E_2$ are about 2.8 ~ 2.9 nm. Given the shell thicknesses of 12 nm and 6 nm, respectively, (Table 2), we can infer that $C_4AzoOC_4E_2$ forms vesicles with shells consisting of four layers, while $C_4AzoOC_6E_2$ forms normal bilayer vesicles.

In contrast, the SANS spectra for the cis isomer were fitted well by the Debye-Anderson-Brumberger (DAB) model[15], which characterizes the scattering density function in random two phase systems, in which two phases with different SLDs randomly penetrate each other and spread over the whole sample. One typical fitting result is shown in Figure 8, in which the correlation length was found to be about 200 nm.

G. Cryogenic Transmission Electron Microscopy (Cryo-TEM)

Typical TEM images for the trans and cis surfactant solutions are shown in Figure 9.

In the trans $C_4AzoOC_6E_2$ 0.6 mM sample, many spherical objects with diameters ranging from 50 to 70 nm were observed in the replica cryo-TEM picture (Figure 9 (a)), indicating that these surfactants self-assembled into spherical aggregates of size similar to that inferred from the SANS analyses. Furthermore, in the vitrified cryo-TEM picture of the same system (Figure 9 (b)), vesicle-like structures were clearly evident. The cryo-TEM images are consistent with the results of the SANS analysis, which indicated that trans $C_4AzoOC_6E_2$ self-assembles into vesicles. In the cryo-TEM

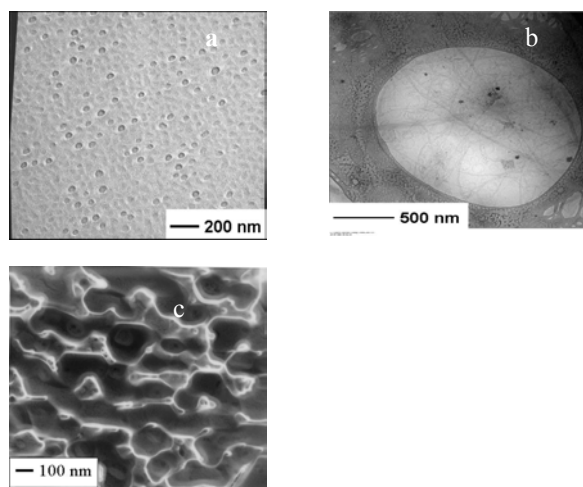


Fig. 9. Cryo-TEM images of photoresponsive surfactant aggregates. (a) Replica, trans $C_4AzoOC_6E_2$ 0.6 mM. (b) Vitrified, trans $C_4AzoOC_6E_2$ 0.6 mM (c) Replica, cis $C_4AzoOC_6E_2$ 0.6 mM.

picture of the cis $C_4AzoOC_6E_2$ solution (Figure 9 (c)), there appear to be many domains of random shape and various sizes. Each domain is enclosed by a wall consisting of surfactants. This structure is consistent with that of a bicontinuous phase. Moreover, the average domain size

was found to be around 200 nm, which is close to the correlation length extracted from the SANS spectra.

H. Neutron reflection

The measured reflectivities are shown in Figure 10. In NRW, reflectivities from the trans and cis isomers, in either azobenzene-deuterated or spacer-deuterated species, were essentially parallel with each other in the low Q range. A similar situation occurred in D_2O . This tendency is consistent with scale analysis. In the small Q range, the spatial resolution of neutron reflection is much larger than the thickness of the adsorbed layer. Under such circumstances, neutrons only “saw” the structure-less thin layer, and all behaved similarly. In NRW, the difference in the magnitudes of the reflectivities comes from the different surface concentrations and SLDs of these deuterated species. In D_2O , because the interface SLD is dominated by D_2O , reflectivities from different species are very close to each other. For Q greater than 0.1 \AA^{-1} , reflectivities from the two deuterated samples (both trans and cis isomer) begin to deviate from each other, with this deviation becoming more pronounced with increasing Q. This deviation in the large Q range was even more obvious in D_2O than in NRW. These deviations in the reflectivities imply that the azobenzene and spacer groups, in both trans and cis form, have different spatial distributions and interfacial positions within the adsorbed layer. The

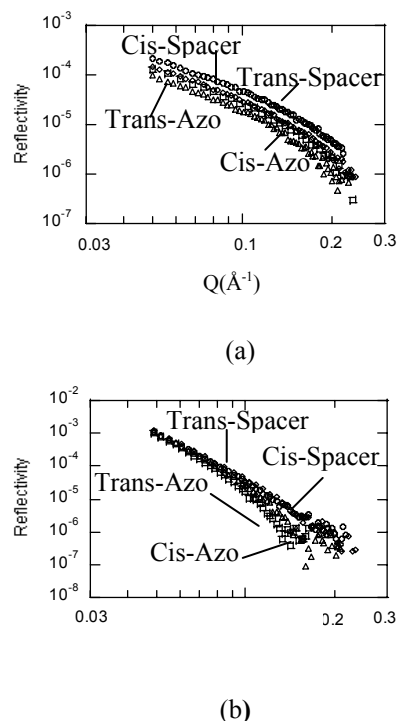


Fig. 10. Measured reflectivities in trans and cis $C_4AzoOC_6E_2$ are plotted together in (a), zero contrast solvent, and in (b) D_2O . Spacer indicates spacer deuterated species, and azo indicates azobenzene deuterated species.

experimental reflectivities of both trans and cis were fitted by a kinematics approximation. The fitting results are plotted in Figure 11 and Figure 12.

IV. DISCUSSION

As shown in the density profiles, Figure 11 (b) and Figure 12 (b), head groups of both trans and cis isomers were almost totally immersed into the bulk water phase, and their hydrophobic moieties such as azobenzene and the spacer group are mostly exposed to the air. This conclusion fits well with the conventional picture of surfactant at the interface, and is consistent with the hydrophilic and hydrophobic nature of the various segments.

For the cis isomer, the positions of all segments have large standard deviations, indicating the intense fluctuations at the interface. This agrees with the large molecular area obtained from the Gibbs equation. Segment distributions in Figure 11(b) reveal one striking feature in the interfacial conformation of the cis isomer. The relative distance between the azobenzene and the spacer group was only 1.5 Å. If this is compared with their standard deviations (6.0 Å for the azobenzene group and 3.35 Å for the spacer), it can be concluded that distributions of azobenzene and spacer group overlap. This quantitative structural information on segment distributions excludes the possibility of a regular vertical conformation, and strongly supports a loop conformation taken by the cis isomer at the interface, in which the surfactant head is immersed in the water sub-phase, and the spacer loops out from the interface with both ends anchored at the interface. As a result, the azobenzene group is also located at almost the same position as the spacer, and its segment distribution overlaps with that of the spacer. The resultant segment distributions for the trans isomer are shown in Figure 12 (b). All segmental distributions show only minor variations at the two ends of the segment. Most parts of the segment are fixed in place. The optimal equilibrium tilt angles and corresponding angle fluctuations are very small for all segments, such as the azobenzene, the spacer, and the head group, are essentially perpendicular to the air-water interface. In contrast to the cis isomer, the trans azobenzene group was well separated from the spacer with a relative distance as large as 7.0 Å. It can be concluded that the azobenzene group lies completely within the air phase and perpendicular to the air-water interface. Based on the above analysis, it can be concluded that trans isomer takes a vertical conformation at the interface.

The neutron reflection results confirmed the hypothesis that the changes in the surface tensions may be ascribed to the orientation and conformation of the surfactants at the air-liquid interface, which are the result of complex interactions between the head and tail groups, both with each other and with the water sub-phase. The appearance of polar groups like the ether oxygen within the tail can lead to a “loop conformation” because of the preferred interactions of these middle polar groups with the

water at the interface. In this configuration, the spacer between the polar head group and the

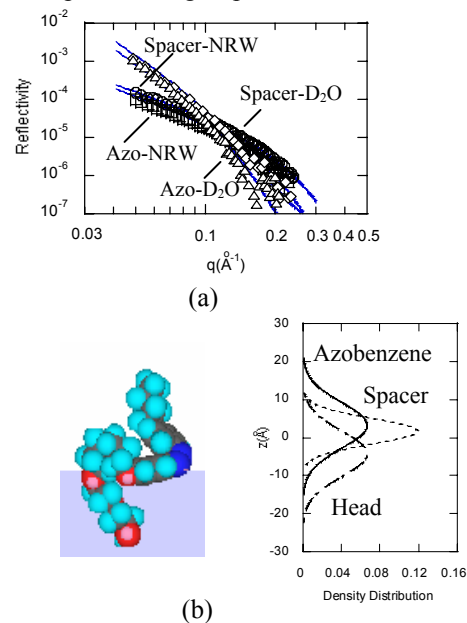


Fig. 11. The curve fitting of neutron reflectivities for cis $C_4AzoOC_6E_2$ (a) and corresponding segmental density distribution (b). In (a), solid lines represent model fitting. “Spacer” and “azo” refer to the spacer and azobenzene deuterated species, respectively. NRW and D_2O indicate the NRW solvent and D_2O , respectively.

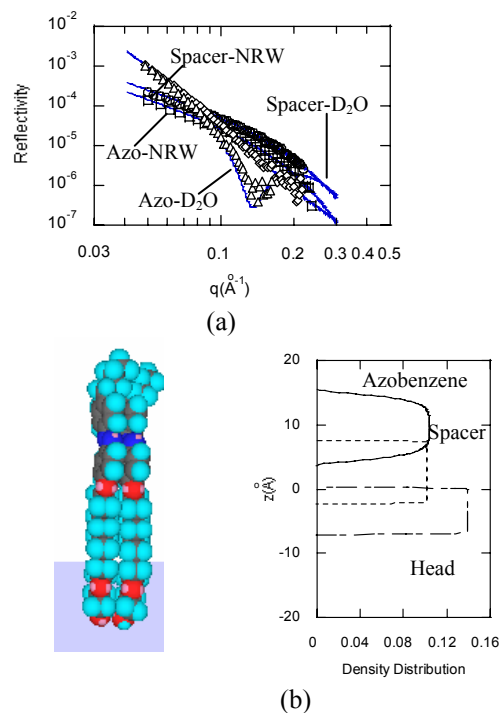


Fig. 12. The curve fitting of neutron reflectivities in trans $C_4AzoOC_6E_2$ (a) and corresponding segmental density distribution (b). In (a), solid lines represent model fitting. Spacer and azo mean the spacer and azobenzene deuterated species, respectively. NRW and D_2O indicate the NRW solvent and D_2O , respectively.

intermediate polar group forms a loop anchored at both ends in the interfacial plane, or lies within the interface. The “loop conformation” of the surfactant also depends on the conformational states of the azobenzene groups themselves, and their interactions with the polar interface, since the localization of the middle polar group at the interface would necessarily cause the azobenzene group to lie in, or be in close proximity and at some angle to, the interfacial plane. If these interactions are sufficiently unfavorable then they will negate the advantages gained by localizing the intermediate polar group at the interface, hence inhibiting formation of the loop, and the preferred configuration would be to have both the spacer and polar group oriented away from the interface. The cis form of the azobenzene group has a folded state with a high dipole moment of 3.1 Debye, while the trans state is planar and has a significantly lower dipole moment of 0.5 Debye. The cis form, in allowing one of the benzene rings to bend away from the interface, reduces unfavorable hydrophobic interactions with the sub-phase. Moreover, the significant dipole moment of the cis conformation of the azobenzene group allows for favorable interactions with the interface; whereas, for the trans conformation, such strong dipole interactions are absent. It is the balance between these different energetic contributions that determines the ultimate conformation at the interface. In the surfactant C₄AzoOC₆E₂, spacers are sufficiently long and flexible that they are capable of forming loops if energy considerations favor this configuration. The trans surfactant adopts an orientation normal to the interface, however, probably stabilized by π - π interactions[16], as indicated by the high interaction enthalpies. The reduction in the stabilizing π - π interactions when the azobenzene group adopts the cis conformation, on the other hand, coupled with its strong dipole moment, favors a configuration where the azobenzene group is partially in the interfacial plane and the spacer loops over the interface.

The azobenzene group in C₄AzoOC₆E₂ is believed to be responsible for the unusual properties in its trans micelles, because of the highly orientation-dependent π - π interaction between them, which essentially originates from the large π -orbital in the benzene. The π - π interaction is strongest when two azobenzene groups are oriented in parallel, and gradually decreases with the change in their relative orientation. It becomes weakest when azobenzenes are perpendicular to each other. Therefore, the π - π interaction exerts a significant effect on micellar packing geometry. It prefers the low curvature micellar structure and induce strong micellar growth phenomena. Simultaneously, at high concentrations, the light-induced bilayer-bicontinuous phase transition can be attributed to the surfactant conformation change because of the azobenzene photoisomerization. According to the Petrov-Derzhanski-Mitov (PDM) model, trans surfactant, whose cross sectional area for the head is larger than for the tail, will have negative Gaussian rigidity, and self-assemble into bilayers; while the cis surfactant, whose cross sectional area for the head is smaller than that for the tail, will have

positive Gaussian rigidity, and self-assemble into a bicontinuous phase.

V. CONCLUSIONS

We have reported on the synthesis and characterization of a new class of nonionic, photo-sensitive surfactants, some of whose trans and cis isomers exhibit unusually large differences in surface properties. For example, in aqueous solutions of these photoresponsive surfactants below their CMCs, surface tension can increase by as much as 28.6 mN/m under UV illumination. More importantly, the difference between saturated surface tensions (at concentrations above their CMCs) was as high as 11.0 mN/m under radiation of different wavelengths. These surfactants are potentially useful in a variety of surface tension related applications, including the control of spreading processes, Marangoni flows and fluid movement in microfluidic devices. Experimental results from neutron reflection revealed that, under certain circumstances, surfactant can take an unusual “loop conformation” at the interface and both the azobenzene and the intermediate polar group play important roles in the control of surfactant conformation and hence surface tension. A molecular interpretation of these phenomena suggests some important principles for the design of such photoresponsive surfactant systems.

The study of self-assembly properties of these photoresponsive surfactants indicates that trans C₄AzoOC₆E₂ exhibits a strong tendency for “micellar growth” as a result of highly orientation-related π - π interactions between azobenzene groups. At high concentrations, there is a remarkable structural transition from the bilayer to the bicontinuous phase when illumination condition is switched from visible light to UV light. This light regulated structural transition originates from the change in molecular architectures accompanying trans-cis isomerization, which changes the sign of Gaussian rigidity.

ACKNOWLEDGEMENT

This work was supported by the Singapore-MIT Alliance.

REFERENCES

- [1] P. C. Hiemenz and R. Rajagopalan, *Principles of Colloid and Surface Chemistry*, 3rd ed. New York: Marcel Dekker, Inc., 1997.
- [2] M. Grunze, *Science*, vol. 283, pp. 41-42, 1999.
- [3] T. Hayashita, T. Kurosawa, T. Miyata, K. Tanaka, and M. Igawa, "Effect of Structural Variation within Cationic Azo-Surfactant Upon Photoresponsive Function in Aqueous-Solution," *Colloid Polym. Sci.*, vol. 272, pp. 1611-1619, 1994.
- [4] L. Yang, N. Takisawa, T. Hayashita, and K. Shirahama, "Colloid-Chemical Characterization of the Photosurfactant 4-

- Ethylazobenzene 4'-
(Oxyethyl)Trimethylammonium Bromide," *J. Phys. Chem.*, vol. 99, pp. 8799-8803, 1995.
- [5] H. Durr, in *Photochromism: Molecules and Systems, Studies in Organic Chemistry*, H. Durr and H. Bousa-Laurent, Eds. Amsterdam: Elsevier, 1990, pp. 1-14.
- [6] N. L. Abbott, L. I. Jong, and J. Y. Shin, "Nonequilibrium, interfacial properties of aqueous solutions of bolaform surfactants containing disulfide and azobenzene groups," *Abstr. Pap. Am. Chem. Soc.*, vol. 218, pp. 16-COLL, 1999.
- [7] A. Anastopoulos and I. Moutziz, "A Contribution to the Study of the Inhibited Electroreduction of Organic-Compounds in Anhydrous Solvents at High Electrode Coverages by Neutral Surfactants - the Reduction of Azobenzene in Methanol as a Model Reaction," *J. Electroanal. Chem.*, vol. 294, pp. 143-150, 1990.
- [8] R. T. Buwalda, J. M. Jonker, and J. Engberts, "Aggregation of azo dyes with cationic amphiphiles at low concentrations in aqueous solution," *Langmuir*, vol. 15, pp. 1083-1089, 1999.
- [9] H. C. Kang, B. M. Lee, J. Yoon, and M. Yoon, "Synthesis and surface-active properties of new photosensitive surfactants containing the azobenzene group," *J. Colloid Interface Sci.*, vol. 231, pp. 255-264, 2000.
- [10] J. Eastoe, M. S. Dominguez, P. Wyatt, A. Beeby, and R. K. Heenan, *Langmuir*, vol. 18, pp. 7837-7844, 2002.
- [11] T. Shang, K. Smith, and T. Hatton, "Photoresponsive surfactants exhibiting unusually large, reversible surface tension changes under varying illumination conditions," *Langmuir*, vol. 19, pp. 10764-10773, 2003.
- [12] E. H. Lucassen-Reynders, in *Anionic Surfactants: Physical Chemistry of Surfactant Action*, vol. 11, E. H. Lucassen-Reynders, Ed. New York: Marcel Dekker, Inc., 1981, pp. 1-54.
- [13] J. S. Higgins and H. C. Benoît, *Polymers and Neutron Scattering / and*, vol. 8. Oxford: Clarendon Press, 1994.
- [14] P. Bartlett and R. H. Ottewill, "A Neutron Scattering Study of the Structure of a Bimodal Colloidal Crystal," *J. Chem. Phys.*, vol. 96, pp. 3306-3318, 1992.
- [15] R. J. Roe, *Methods of X-ray and Neutron Scattering in Polymer Science*. New York: Oxford University Press, 2000.
- [16] D. G. Whitten, L. H. Chen, H. C. Geiger, J. Perlstein, and X. D. Song, *J. Phys. Chem. B*, vol. 102, pp. 10098-10111, 1998.

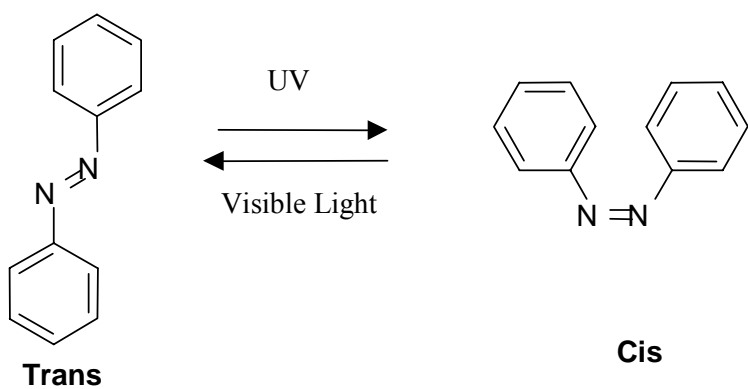


Fig. 1. Photoisomerization of azobenzene.

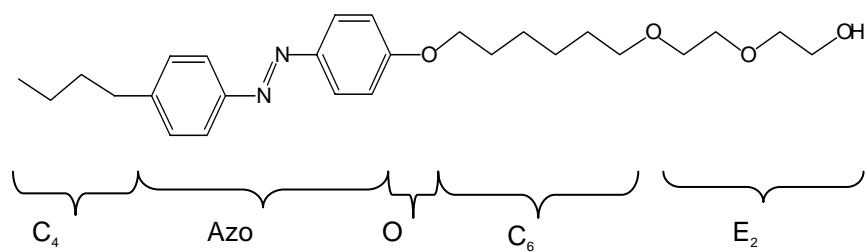


Fig. 2. Molecular structure of photo-responsive surfactants $C_4AzoOC_nE_2$; the structure for $n = 6$ is shown. C_4 = butyl tail group; Azo = azobenzene group; O = ether oxygen middle polar group; C_6 = alkyl spacer with 6 methylene groups; E_2 = surfactant head group consisting of two ethylene oxide moieties.

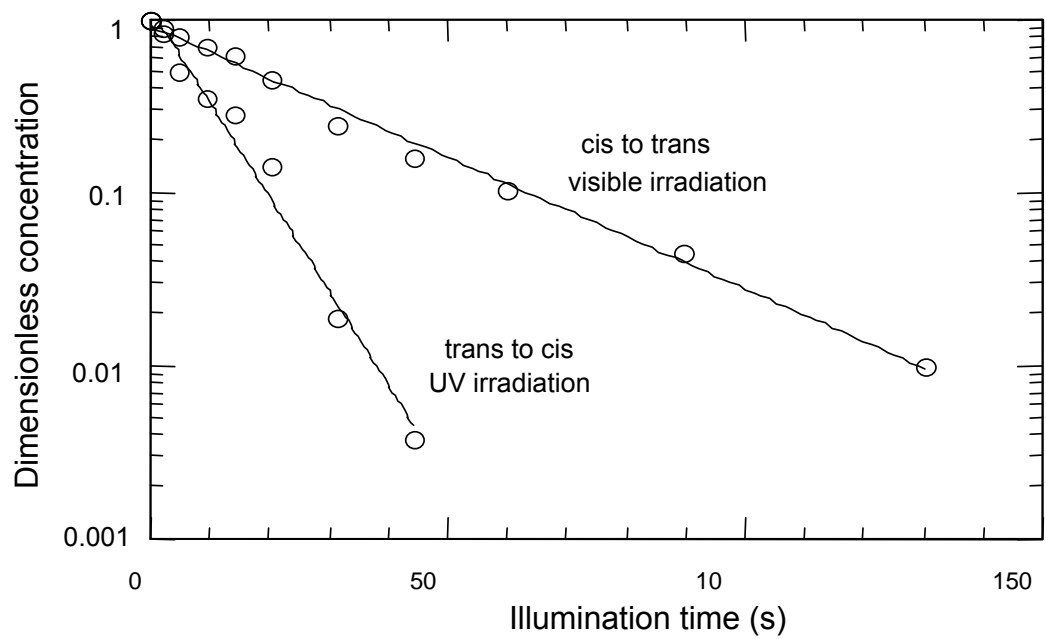
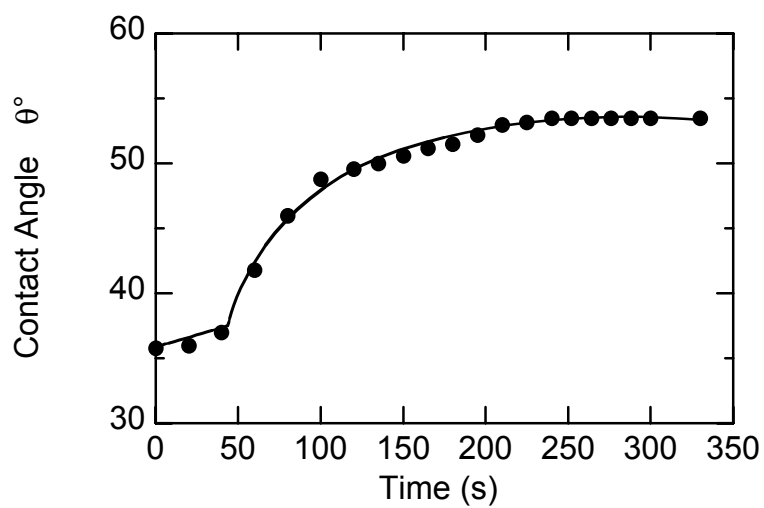
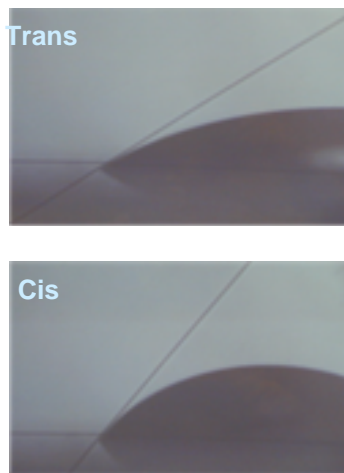


Fig. 3. Kinetics of photo-isomerization in $C_4AzoOC_6E_2$ solutions for the trans-to-cis and cis-to-trans processes under similar irradiation intensities. Solid lines represent least squares fits of the kinetic model to the data.



(a)

(b)

Fig. 4. Contact angle changes for droplets of $C_4AzoOC_6E_2$ solutions (0.07 mM) on a hydrophobic surface under different illumination conditions (visible illumination for the trans isomer, UV illumination for the cis isomer). The time-course of contact angle variation under UV illumination is shown.

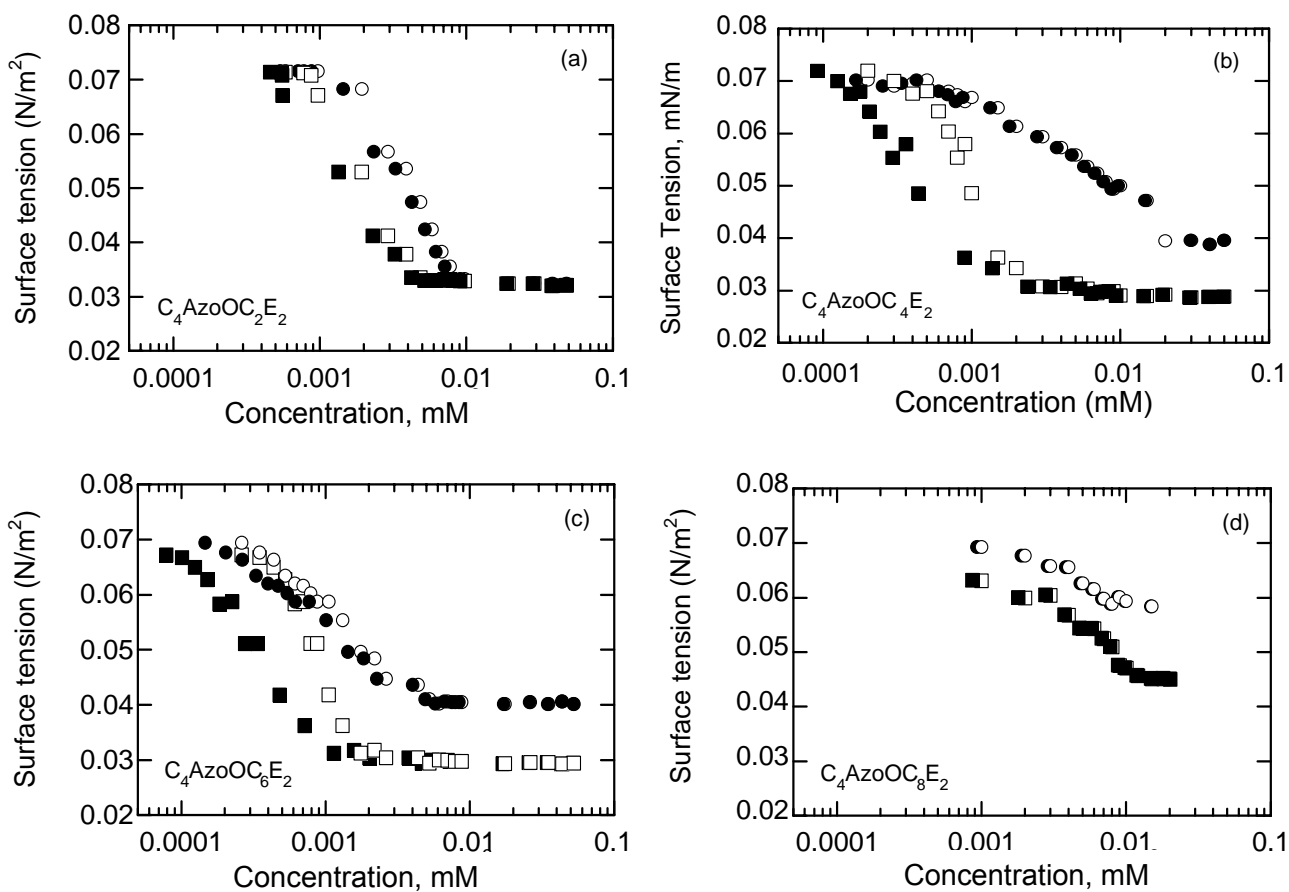


Fig. 5. Concentration dependence of the equilibrium surface tension for photoresponsive surfactants at 25 °C under both visible (squares) and UV light (circles) illumination. The open symbols represent the original data as a function of the nominal, as-prepared concentration; the solid symbols represent data corrected for interfacial adsorption to give the true bulk concentration. (a) $C_4AzoOC_2E_2$ (b) $C_4AzoOC_4E_2$ (c) $C_4AzoOC_6E_2$ (d) $C_4AzoOC_8E_2$

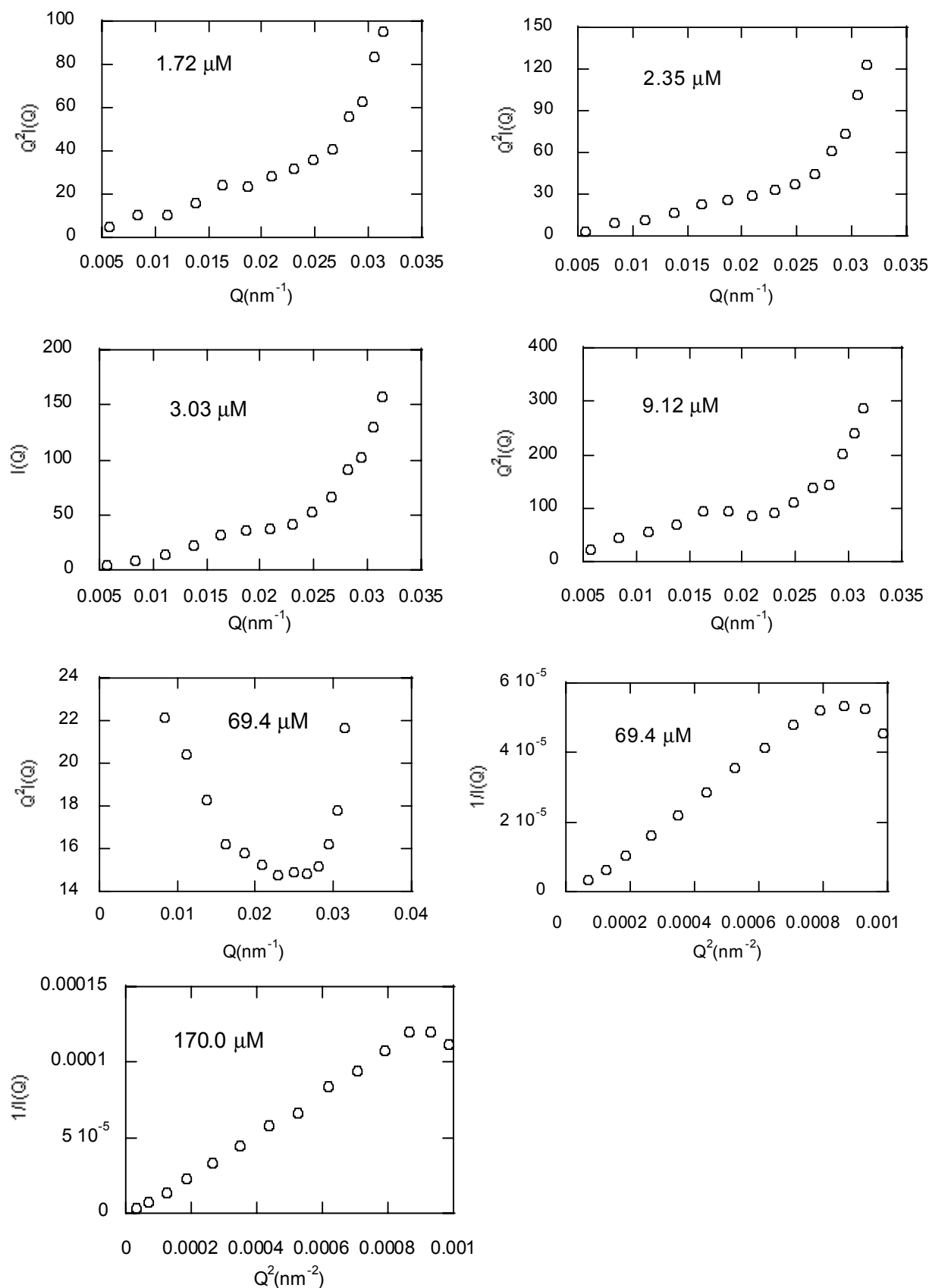


Fig. 6. Light scattering results of $\text{C}_4\text{AzoOC}_6\text{E}_2$. The scattering results are plotted in Kratky Plot for samples of 1.72, 2.35, 3.03, and 9.12 μM , and in Zimm Plot for 69.4 and 170.0 μM samples.

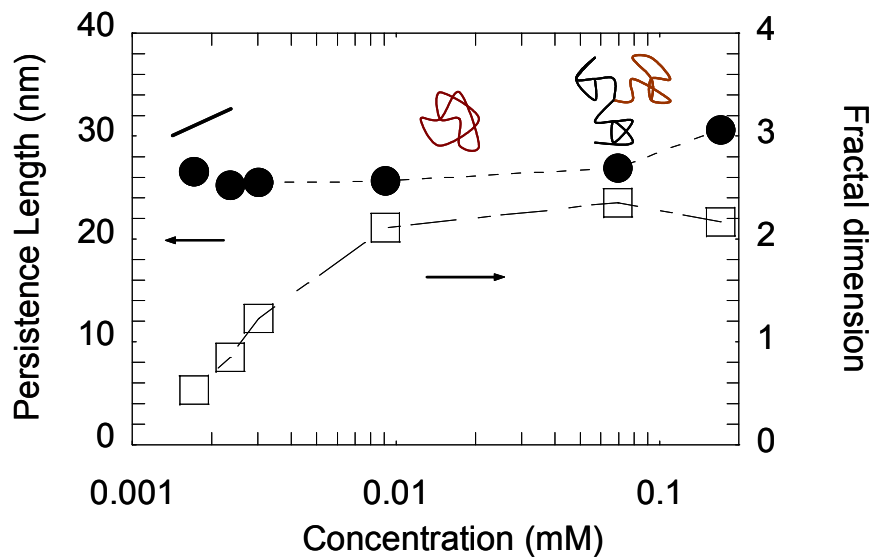


Fig. 7. Summary of static light scattering (SLS) results for trans $C_4AzoOC_6E_2$.

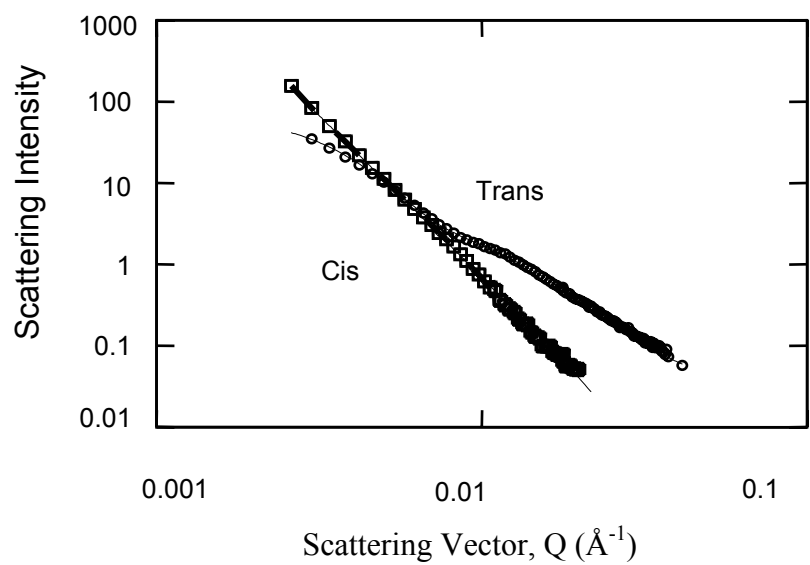


Fig. 8. Small angle neutron scattering results of $C_4AzoOC_6E_2$ 0.6 mM. Open symbols are the experimental data. Solid lines represent the model fitting of scattering intensities.

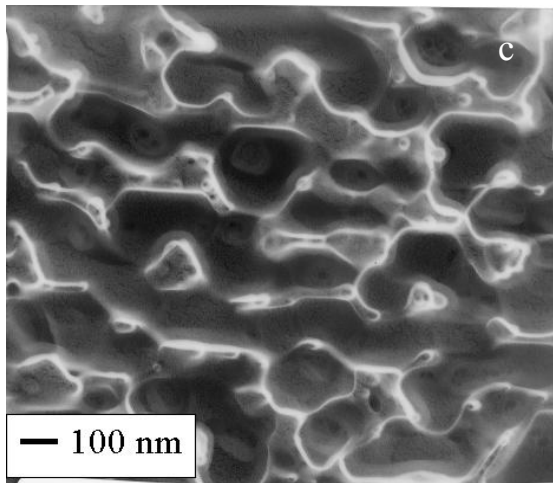
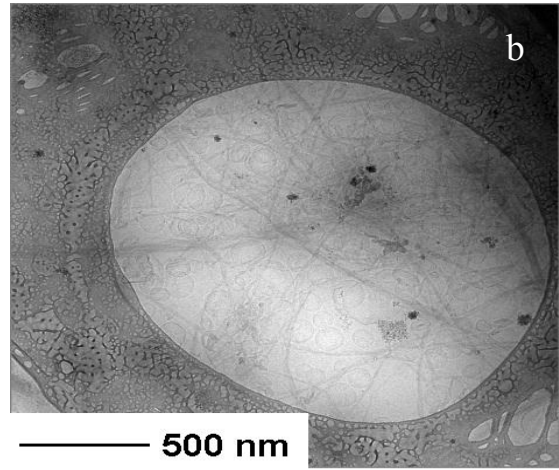
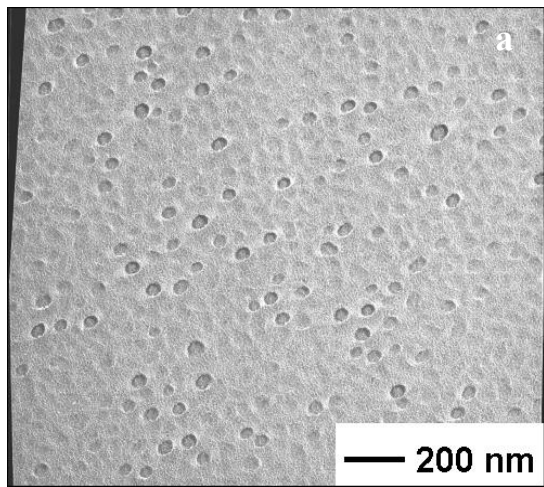


Fig. 9. Cryo-TEM images of photoresponsive surfactant aggregates. (a) Replica, trans $C_4AzoOC_6E_2$ 0.6 mM. (b) Vitrified, trans $C_4AzoOC_6E_2$ 0.6 mM (c) Replica, cis $C_4AzoOC_6E_2$ 0.6 mM.

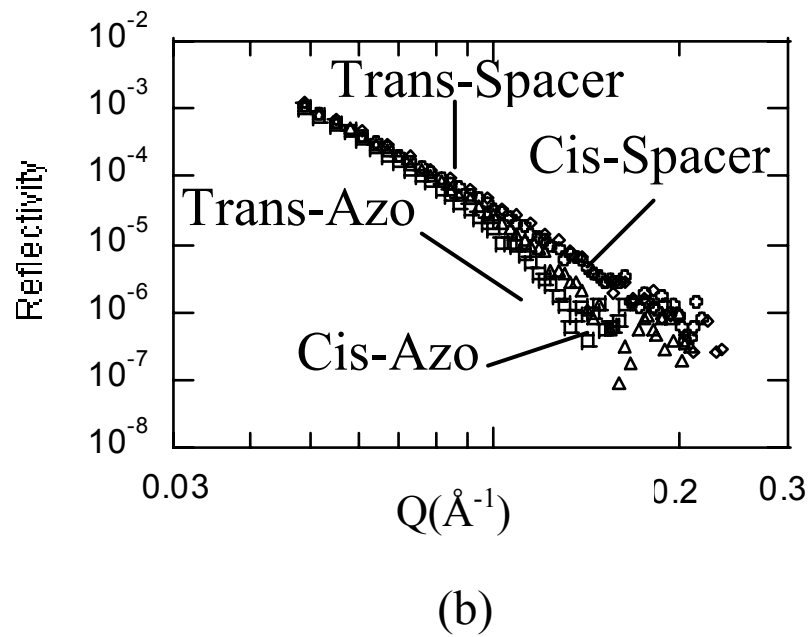
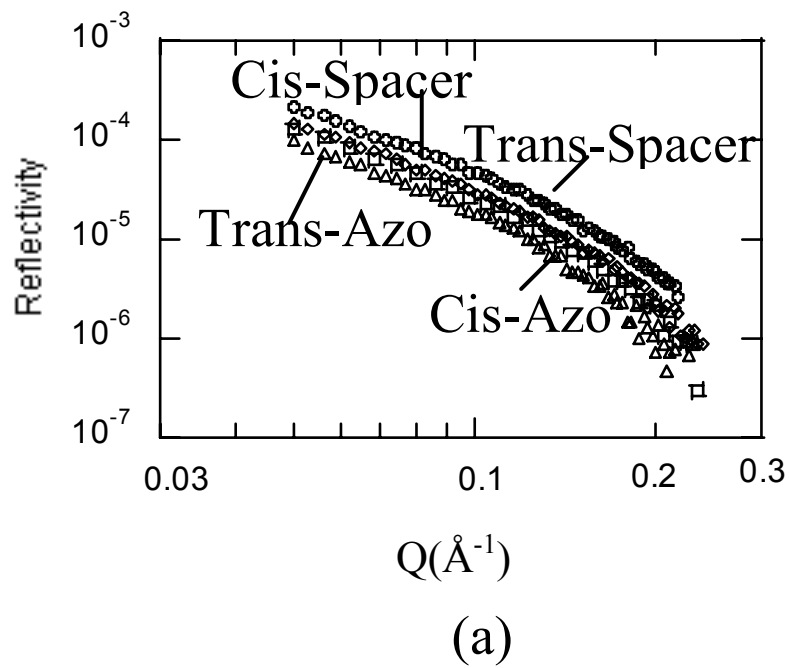


Fig. 10. Measured reflectivities in trans and cis $C_4AzoOC_6E_2$ are plotted together in (a), zero contrast solvent, and in (b) D_2O . Spacer indicates spacer deuterated species, and azo indicates azobenzene deuterated species.

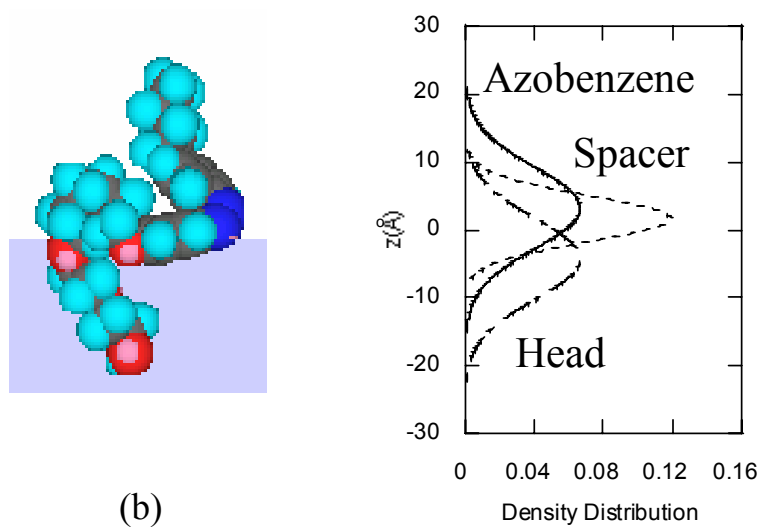
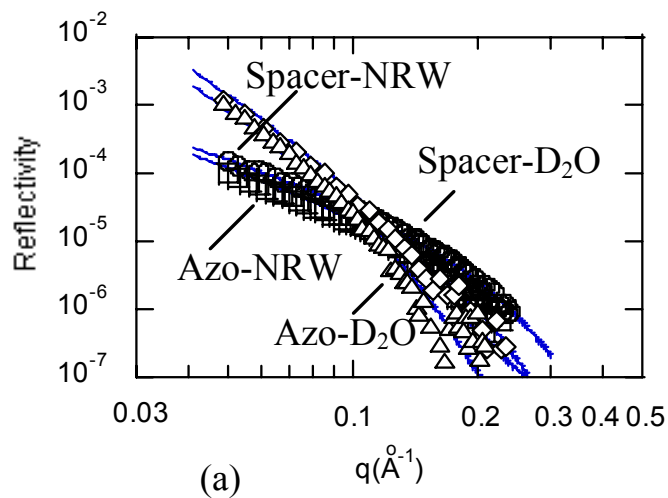
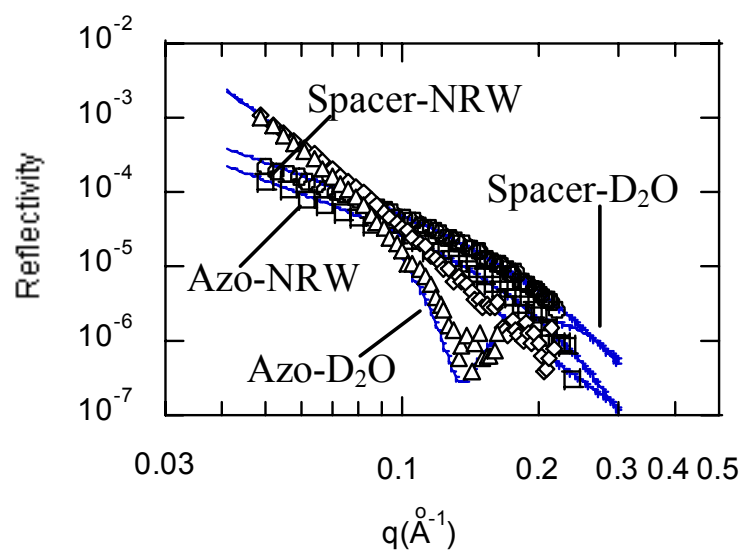
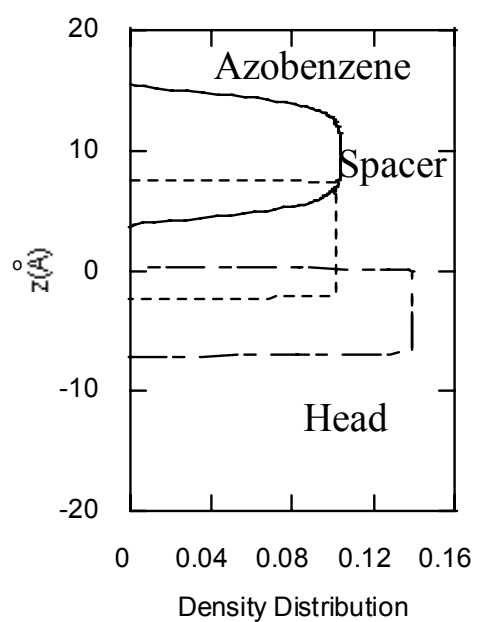
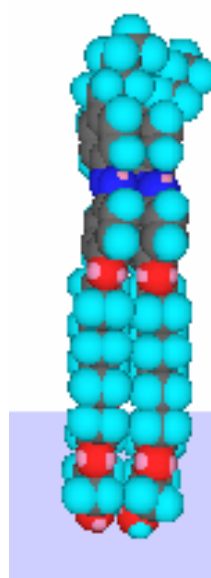


Fig. 11. The curve fitting of neutron reflectivities for *cis* C₄AzoOC₆E₂ (a) and corresponding segmental density distribution (b). In (a), solid lines represent model fitting. Spacer and azo refer to the spacer and azobenzene deuterated species, respectively. NRW and D₂O indicate the NRW solvent and D₂O, respectively.



(a)



(b)

Fig. 12. The curve fitting of neutron reflectivities in trans $C_4AzoOC_6E_2$ (a) and corresponding segmental density distribution (b). In (a), solid lines represent model fitting. Spacer and azo mean the spacer and azobenzene deuterated species, respectively. NRW and D_2O indicate the NRW solvent and D_2O , respectively

TABLE 1
Summary of Light Scattering Results.

Concentrations (mM)	Persistence length (nm)	Fractal dimension
1.72×10^{-3}	26.6	0.53
2.35×10^{-3}	25.2	0.85
3.02×10^{-3}	25.5	1.23
9.12×10^{-3}	25.6	2.11
69.4×10^{-3}	26.9	2.35
170.4×10^{-3}	30.6	2.17

TABLE 2
Fitting Parameters of SANS in Trans Samples.

	$C_4AzoOC_4E_2$		$C_4AzoOC_6E_2$
Concentration (mM)	0.7	1.2	0.6
Average vesicular radius (nm)	38.41	43.5	28.08
Shell thickness (nm)	11.24	12.5	5.85
Polydispersity	0.43	0.37	0.74